

Boron Nitride as a Selective Gas Adsorbent

Jurik F. Janik, William C. Ackerman, Robert T. Paine, Duen-Wu Hua,
Alok Maskara, and Douglas M. Smith*

Department of Chemistry, Department of Chemical and Nuclear Engineering, and the
UNM/NSF Center for Micro-Engineered Ceramics, University of New Mexico,
Albuquerque, New Mexico 87131

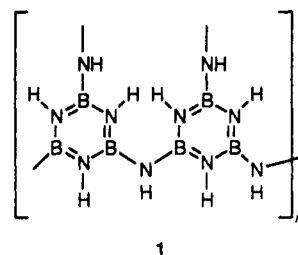
Received September 16, 1992. In Final Form: November 5, 1993*

A series of eight porous boron nitride materials with nitrogen/BET surface areas of 437–712 m²/g have been produced using polymeric precursors varied by systematic synthesis modifications. All samples exhibit type I isotherms indicating that a majority of the porosity occurs in pores with radius less than 1.0 nm. Carbon dioxide adsorption at 273 K was analyzed using the Dubinin–Radushkevich (D–R) and Dubinin–Astakov (D–A) equations. Significant differences between BET/N₂ and D–R/CO₂ surface areas are observed. Adsorption of carbon dioxide and methane is measured at 273 K over the pressure range of 0–800 Torr, and significant differences in adsorption selectivity are observed. Although all eight samples have similar BET surface areas, the carbon dioxide uptake at 273 K and 800 Torr varies from 9.5 to 125 cm³/g. Differences in the chemical and physical structure of the samples are probed with Fourier transform IR, X-ray diffraction, and small angle X-ray scattering measurements. CH₄/CO₂ selectivity correlates with both the radius of gyration obtained from SAXS and the D–A coefficient from CO₂ adsorption.

Introduction

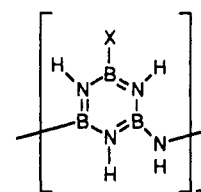
Activated carbon materials are employed in many gas and liquid phase industrial processes to remove impurities. In most cases, impurity binding to the carbon surface occurs through an adsorptive interaction, and some of the factors that influence the adsorptive strength and capacity of a given material have been studied.¹ In particular, it appears that surface area, pore structure, surface polarity, and activation processing parameters all play a significant role in determining the efficacy of a given material in a specific separation. Despite this knowledge, it is still not possible to rationally tailor surface area, microporosity, and surface polarity conditions in order to solve new separation problems. However, recent progress in polymer synthesis and processing may provide approaches to accomplish this goal.

One carbon-like material that has potential for adsorption applications is boron nitride. BN has a graphite-like structure related to the structure of carbon, but the nature of the individual B–N bonds introduces local polar character not present in the carbon structure. Since polar sites are considered to improve adsorption,¹ we anticipate that porous BN may be a good adsorbent. In practice, commercial, metallurgically prepared BN samples have low surface areas.² This renders them relatively useless for adsorption applications.³ We have previously observed that BN samples produced from poly(2,4,6-borazinylamine) (1) have surface areas in the range of 30–50 m²/g for powders produced at 900 °C,³ and these materials also would not be expected to be useful. On the other hand, boron nitride aerogels formed by critical point drying of poly(2,4,6-borazinylamine) gels and heated to 1000 °C exhibit low density, are highly porous, and have surface areas of ~400 m²/g.⁴ These materials adsorb H₂, O₂, CO₂, and CO;⁵ however, as with most aerogels, the porosity is



1

primarily mesoporosity.⁴ In another approach, it was reasoned that a polymer with two sites involved in ring condensation should result in a more compliant (i.e., lower pore volume) polymer network after drying. Indeed, boron nitride samples with surface areas of 53–696 m²/g and pore volumes of 0.036–0.390 cm³/g were produced by vacuum pyrolysis of poly(4,6-borazinylamine) (2) poly-



2

merized under dilute conditions.⁷ Surface area and pore volume were maximized at pyrolysis temperatures of 800 °C and essentially eliminated by 1200 °C. These previous results^{4–7} indicate that the pore structure of polymer-derived boron nitride is a function of both the precursor polymer structure and pyrolysis conditions. The demonstration of the ability to tailor BN pore structure and adsorption properties via the controlled variation of these parameters is an important advance in nonoxide prece-

* Author to whom correspondence should be addressed.

† Abstract published in *Advance ACS Abstracts*, January 15, 1994.

(1) Bansal, R. C.; Donnet, J.-B.; Stoeckli, F. In *Active Carbon*; Marcel Dekker, Inc.: New York, 1988.

(2) Technical Data Sheet, Boron Nitride, ESK Engineered Ceramics Wacker Chemicals (USA) Inc.

(3) Narula, C. K.; Schaeffer, R.; Paine, R. T.; Datye, A.; Hammett, W. F. *J. Am. Chem. Soc.* 1987, 109, 5556–5557.

(4) Lindquist, D. A.; Borek, T. T.; Kramer, S. J.; Narula, C. K.; Johnston, G.; Schaeffer, R.; Smith, D. M.; Paine, R. T. *J. Am. Ceram. Soc.* 1990, 73 (3), 757–760.

(5) Lindquist, D. A. PhD Thesis, University of New Mexico, 1990; p 67–78.

(6) Narula, C. K.; Schaeffer, R.; Datye, A. K.; Borek, T. T.; Rapko, B. M.; Paine, R. T. *Chem. Mater.* 1990, 2, 384–389.

(7) Borek, T. T.; Ackerman, W.; Hua, D. W.; Paine, R. T.; Smith, D. M. *Langmuir* 1991, 7, 2844–2846.

ramic polymer processing. Our continuing systematic studies of these features are described here.

Experimental Section

Synthesis of BN Samples. All reagents and polymers were handled under a dry nitrogen atmosphere by using Schlenk glassware and a dual manifold vacuum/inert atmosphere system. All solvents were dried with appropriate reagents and distilled prior to use. Polymer pyrolysis was accomplished with a horizontal tube furnace, and samples were contained in quartz or platinum crucibles inside a quartz tube in which the pyrolysis atmosphere could be varied.

Sample a. A sample of $(\text{Me}_2\text{NB})\text{B}_2\text{Cl}_2\text{N}_3\text{H}_3$ (3.28 g, 17.0 mmol)⁸ was dissolved in 120 mL of chlorobenzene and $(\text{Me}_3\text{Si})_2\text{NH}$ (2.74 g, 17.0 mmol) was added via syringe to the stirred solution held at 23 °C. The mixture formed a gel that contained some of the solvent. The solvent was vacuum evaporated, and the remaining solid was vacuum dried for 24 h. The residue (3.12 g) was treated twice with 150 mL of $\text{NH}_3(\text{l})$ held at ~ -30 °C and allowed to stand for 4–5 h with a slow stream of N_2 passing through the flask. The $\text{NH}_3(\text{l})$ slowly evaporated under these conditions. During this process, the polymer dissolved in the $\text{NH}_3(\text{l})$. The resulting foamy residue (2.7 g) was vacuum dried for 30 min. IR spectrum (KBr, cm^{-1}): 3486 (m), 3416 (m), 3200 (w), 2955 (w), 2928 (w), 2872 (w), 1611 (m), 1478 (s), 1420 (s), 1371 (s), 1192 (w), 1132 (m), 843 (w), 710 (m), 662 (w), 421 (w). Thermal gravimetric analysis (TGA): total weight loss 37%. The polymer was pyrolyzed at 800 °C while the volatile byproducts were removed continuously *in vacuo*. The residue was tan in color. IR (KBr, cm^{-1}): 3435 (w), 1397 (s, br), 797 (m), 617 (w, sh), 527 (w).

Sample b. The polymer was prepared in a fashion analogous to polymer a from $(\text{Et}_2\text{NB})\text{B}_2\text{Cl}_2\text{N}_3\text{H}_3$ ⁹ (6.19 g, 28.1 mmol) and $(\text{Me}_3\text{Si})_2\text{NH}$ (4.53 g, 28.1 mmol). The mixture was stirred at 23 °C for 48 h. A powder was obtained instead of a gel. This was vacuum dried overnight, leaving 6.6 g of dry solid. IR spectrum (KBr, cm^{-1}): 3451 (m), 3325 (w, sh), 2967 (s), 2928 (m), 2872 (m), 1499 (s), 1474 (s), 1360 (s), 1227 (m, sh), 1109 (s), 1018 (w), 968 (w), 914 (w), 839 (m), 714 (s), 619 (s), 538 (w). A portion of this solid (2 g) was placed in a Schlenk vessel and contacted with two portions of $\text{NH}_3(\text{l})$ (120 mL each) at -30 °C. The $\text{NH}_3(\text{l})$ was left in contact with the polymer for a total of 8 h, and the polymer showed a small solubility in $\text{NH}_3(\text{l})$. The $\text{NH}_3(\text{l})$ was allowed to slowly evaporate from the container. IR (KBr, cm^{-1}): 3488 (w), 3420 (s), 3204 (w), 2967 (m), 2930 (w), 2872 (w), 2484 (w, br), 1611 (m), 1495 (s), 1371 (s), 1194 (w), 1127 (m), 1024 (w), 984 (w), 839 (m), 710 (s), 633 (m), 405 (w). TGA: total weight loss 35%. The resulting polymer was pyrolyzed *in vacuo* at 1000 °C for 14 h. The remaining residue (tan) was slightly agglomerated. IR (KBr, cm^{-1}): 3437 (w), 1373 (s), 799 (m).

Sample c. A portion of the polymer b was pyrolyzed *in vacuo* at 800 °C for 14 h. The remaining residue (tan) was a free-flowing powder. IR (KBr, cm^{-1}): 3437 (w), 1371 (s), 797 (m), 611 (w), 525 (w). This sample was then heated at 800 °C under a flowing stream of $\text{NH}_3(\text{g})$ for 14 h. The residue was bone colored. IR (KBr, cm^{-1}): 3439 (w), 1373 (s), 801 (m), 679 (w), 617 (w).

Sample d. The polymer was prepared as described for polymer a from $(i\text{-Pr}_2\text{NB})\text{B}_2\text{Cl}_2\text{N}_3\text{H}_3$ ⁹ (2.42 g, 9.7 mmol) and $(\text{Me}_3\text{Si})_2\text{NH}$ (1.57 g, 9.7 mmol) in chlorobenzene. The reaction is slow at 23 °C; consequently the mixture was refluxed for 24 h, and a rigid gel was produced. The solvent was vacuum evaporated for 24 h, and 3.7 g of polymer was obtained. IR (KBr, cm^{-1}): 3480 (w), 3441 (w), 2955 (m), 2924 (s), 2855 (m), 2724 (w), 2490 (w), 1460 (s), 1404 (s), 1377 (s), 1215 (w), 1182 (w), 1154 (w), 1134 (w) 1020 (w), 847 (w), 723 (m), 635 (m), 521 (w). The polymer (3.5 g) was then exposed 3 times to 120 mL of $\text{NH}_3(\text{l})$ at -30 °C for 5 h, and the NH_3 was allowed to slowly boil off during each exposure. The remaining residue was vacuum dried. The solid was then extracted with 90 mL of Et_2O and vacuum dried for 4 h. A sample of this polymer (0.6 g) was pyrolyzed *in vacuo* at 800 °C for 14

h, and a speckled tan/brown solid was obtained (0.32 g). IR (KBr, cm^{-1}): 3441 (w), 1383 (s), 804 (m), 694 (m), 619 (w).

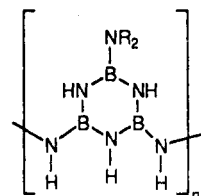
Sample e. Liquid ammonia (~ 120 mL, ~ 5 mol) was condensed into a 300-mL Schlenk vessel fitted with a -78 °C cold finger condenser. The $\text{NH}_3(\text{l})$ was held at -78 °C with an external cold bath, and 3 mL (35 mmol) of BCl_3 was vapor transferred to the flask. The reaction was rapid, so the rate of the addition was controlled by warming and cooling of the BCl_3 storage reservoir. The mixture was stirred briefly in order to wash any white solids formed on dry flask surfaces into the bulk reaction mixture. The NH_3 was then slowly evaporated under a nitrogen gas purge. The polymer formed in this fashion is soluble in $\text{NH}_3(\text{l})$. IR (KBr, cm^{-1}): 3430 (w, sh), 3220 (s), 3080 (s), 2810 (m), 2100 (w, br), 1610 (m), 1410 (s), 1150 (w), 690 (m). TGA: total weight loss 85%. A sample of the polymer was pyrolyzed at 1000 °C *in vacuo* for 14 h. IR (KBr, cm^{-1}): 3437 (w), 2917 (vw), 2849 (vw), 1389 (s), 804 (s).

Sample f. A sample of freshly sublimed $(\text{ClBNH})_3$ (4.0 g, 21.8 mmol) was placed in a Schlenk vessel, and 120 mL of $\text{NH}_3(\text{l})$ was vapor transferred onto the solid at -196 °C.¹⁰ The flask was slowly warmed, and a vigorous reaction took place as the NH_3 liquefied. The system was held at -78 °C for 2 h and then warmed slowly (5 h) to allow NH_3 to escape from the flask. The resulting white solid was vacuum dried overnight, leaving 5.8 g of white solid. IR (KBr, cm^{-1}): 3430 (m), 3210 (s), 3100 (s), 2650 (m), 2100 (w), 1760 (w), 1610 (m), 1570 (m, sh), 1400 (s), 1270 (w), 1080 (m), 650 (m). TGA: total weight loss 72%. A sample of the polymer (1 g) was pyrolyzed *in vacuo* at 1000 °C, and a bone-colored solid was retained. IR (KBr, cm^{-1}): 3429 (w), 1390 (s), 805 (s).

Sample g. A sample of polymer b (2.0 g, 12.1 mmol idealized two-point polymer) was suspended in 60 mL of dry Et_2O , and an aliquot of commercial- $\text{H}_3\text{B}\cdot\text{THF}$ solution (Aldrich, 24.3 mL, 1 M solution) was added from a syringe. The mixture was stirred at 23 °C for 3 days. The mixture was filtered and the residue washed with 30 mL of Et_2O and dried *in vacuo*. IR (KBr, cm^{-1}): 3443 (s), 2961 (m), 2940 (m), 2874 (w), 2511 (w), 1487 (s), 1427 (s), 1387 (s), 1171 (m), 1123 (m), 974 (w), 907 (w), 841 (w), 719 (m), 638 (m). TGA: total weight loss 45%. A portion of this polymer was pyrolyzed at 1000 °C *in vacuo* for 14 h, and a light gray solid was recovered. IR (KBr, cm^{-1}): 3437 (vw), 1381 (s), 806 (m), 538 (w).

Sample h. A sample of polymer a was prepared as described above except that the chlorobenzene solution was refluxed for 14 h. The polymer was isolated by filtration, and it was vacuum dried. A sample of the polymer (3.1 g) was added to 120 mL of $\text{H}_3\text{B}\cdot\text{THF}$ solution (45 mL, 1 M solution) and stirred at 23 °C for 24 h. The slurry was filtered and the solid residue vacuum dried. IR (KBr, cm^{-1}): 3449 (w), 2959 (m), 2938 (m), 2874 (w), 2521 (w), 1495 (s), 1464 (s), 1418 (s), 1387 (s), 1339 (s), 1298 (w, sh), 1179 (m), 1121 (w), 1073 (w), 1034 (w), 974 (w), 910 (w), 713 (m), 665 (w). TGA: total weight loss 75%. A sample of the polymer was pyrolyzed at 800 °C *in vacuo* for 14 h. The solid retained was dark and consequently was pyrolyzed for 14 h at 1000 °C under a stream of $\text{NH}_3(\text{g})$. IR (KBr, cm^{-1}): 3439 (w), 1395 (s, br), 1096 (w), 808 (m), 687 (w), 625 (w).

Sample Organization. Two-point polymers that result in samples a–d form a related set from a chemical/structural standpoint. The idealized structure is represented here.



- 3a: $\text{R}_2\text{N} = \text{Me}_2\text{N}$
 b: $\text{R}_2\text{N} = \text{Et}_2\text{N}$
 c: $\text{R}_2\text{N} = \text{Et}_2\text{N}$
 d: $\text{R}_2\text{N} = i\text{-Pr}_2\text{N}$

Polymers a–c were prepared in an essentially identical fashion. The monomer and hexamethyldisiloxane (HMDS) were allowed

(8) Beachley, O. T., Jr.; Durkin, T. R. *Inorg. Chem.* 1974, 13, 1768–70.
 (9) Rapko, B. M.; Janik, J. F.; Paine, R. T. To be submitted for publication.

(10) Janik, J. F.; Paine, R. T. To be submitted for publication.

to react at 23 °C, and the resulting polymers were treated with $\text{NH}_3(\text{l})$. Polymer **d**, however, was prepared by refluxing the monomer mixture in chlorobenzene. Polymers **a**, **b**, and **d** would be expected to display slightly different room temperature structures as a result of the varying steric demands of the NR_2 groups. Further, the formation of **d** under reflux conditions should result in a more cross-linked, rigid structure. Qualitatively, the physical structures do differ, as evidenced by the gel or powder forms of the materials. Each polymer was treated with $\text{NH}_3(\text{l})$. This chemical treatment serves to cleave off the organic amine fragments in the two-point polymers via a solvolysis reaction, and an amino NH_2 group is substituted in its place. Solvolysis is not complete, as evidenced by weak infrared absorptions in the C-H stretch region ($3000\text{--}2800\text{ cm}^{-1}$).

The pyrolysis schemes for polymers **a**, **b**, and **d** are related. They are pyrolyzed *in vacuo* at 800 °C or 1000 °C. Sample **c** was treated differently in that it was pyrolyzed under NH_3 in order to remove additional organic residue. Infrared spectra of all samples following pyrolysis display a weak absorption in the NH stretch region $3500\text{--}3300\text{ cm}^{-1}$, indicating that the conversion to pure BN is not complete for the entire sample.

Polymers that form samples **g** and **h** also originate from two-point polymers **b** and **a**, respectively. Both polymers have been further treated with $\text{H}_3\text{B}\cdot\text{THF}$. This serves to cleave off the R_2N group and replace it not with an NH_2 group, as described above, but instead with an H atom. The sample of polymer **a** utilized to form sample **h** was obtained from reflux of a chlorobenzene solution of monomer and $(\text{Me}_3\text{Si})_2\text{NH}$. Consequently, the structures of **g** and **h** should be different as well from **a**–**d**.

Polymers **e** and **f** are unique in that they are based on the polycondensation of amino boranes (e.g., the hypothetical species $\text{B}(\text{NH}_2)_3$ and known $(\text{H}_2\text{NBNH})_n$).¹¹ The pyrolyzed samples might be expected to show a more highly cross-linked polymer structure. The pyrolyzed samples display weak N–H vibrations that once more suggest that the materials are not fully converted to BN.

Sample Characterization

Specific surface area, total pore volume, and micropore surface area were determined from N_2 adsorption/condensation at 77 K measured using a Quantachrome Autosorb-1 automated volumetric analyzer. Before analysis, samples were outgassed under vacuum at 350 °C for 3 h. Surface areas were determined by using Brunauer–Emmett–Teller (BET) analysis (five points, $0.05 < P/P_0 < 0.20$) and a molecular cross-sectional area of 0.162 nm^2 . Micropore surface areas were estimated by using deBoer's *t*-plot analysis.¹² Carbon dioxide uptake at 196 K was measured over the relative pressure range of 10^{-5} to 0.99 using a Micromeritics ASAP-2000M adsorption analyzer equipped for low pressure measurements. Adsorption of carbon dioxide and methane (all UHP) was measured at 273 K over the pressure range of 0–800 Torr using a Micromeritics ASAP-2000 automated volumetric analyzer and the same outgassing procedure as described above. CO_2 adsorption was analyzed with the Dubinin–Radushkevich (D–R) and Dubinin–Astakhov (D–A) isotherms.¹³

Infrared spectra were recorded from KBr pellets on a Mattson Galaxy Series 2020 FT-IR. X-ray diffraction patterns were collected using a curved position sensitive detector (INEL CPS 120). The X-ray source was a rotating anode generator operating at 40 kV and 40 mA. A collection time of 30 min was used. Background subtraction was used in order to eliminate any effects due to the sample holder. Small angle X-ray scattering (SAXS) data were collected by using a Rigaku-SAXS system having a Kratky U-slit. The incident beam wavelength was 1.54

(11) Kienner, Y.; Kubo, Y.; Hayashi, N. *J. Inorg. Organomet. Polym.* 1992, 2, 231.

(12) deBoer, J. H.; Linsen, B. G.; van der Plus, T.; Zondervan, G. J. *J. Catal.* 1965, 4, 649.

(13) Marsh, H. *Carbon* 1987, 25, 49.

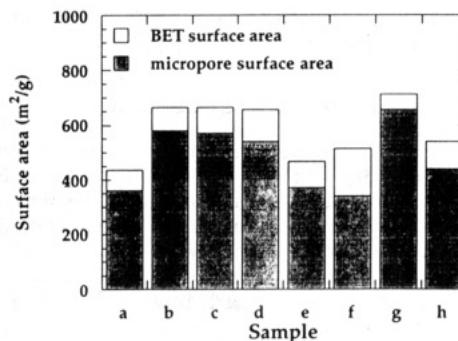


Figure 1. Micropore and total (BET) surface area determined from nitrogen adsorption at 77 K.

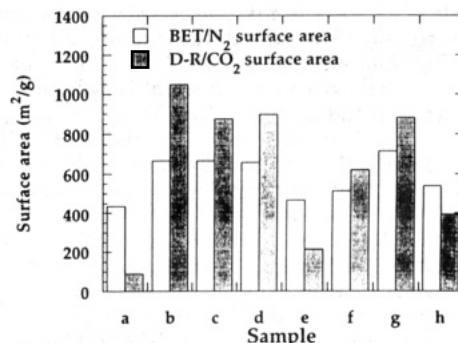


Figure 2. Comparison of BET/ N_2 and D–R/ CO_2 surface areas.

Å of $\text{Cu K}\alpha$ radiation. The intensity of the scattered X-rays was counted with a M. Braun position sensitive detector system. The data were then corrected for the slit collimation in order to evaluate the radius of gyration by the behavior in the Guinier region.

Results and Discussion

The BET surface area and the micropore surface area from *t*-plot analysis for the eight samples is shown in Figure 1. All samples exhibited a large fraction of microporosity and had total (BET) surface areas ranging from 437 to 712 m^2/g . No clear trend in the variation of surface area with polymer precursor structures and/or synthesis/pyrolysis conditions is observed except that two of the lowest values (**a** and **h**) occur for samples prepared from the polymer **a** with the smallest initial NR_2 blocking group. Further, polymers **e** and **f** should be the most highly cross-linked and least compliant and, therefore, would be expected to exhibit lower microporosity.

CO_2 adsorption at 196 K was attempted for several samples. However, equilibrium at a given pressure was not obtained within a time frame which was experimentally accessible (<1 h per point) in our volumetric adsorption apparatus. We have analyzed the 273 K carbon dioxide adsorption isotherms using the D–R isotherm, and the surface area for each sample is reported in Figure 2 and compared to the BET/ N_2 surface areas. A significant variation in the D–R surface area is noted. Perhaps with the exception of sample **f**, samples with the lowest BET surface areas (**a**, **e**, **h**) had D–R surface areas much less than the BET surface area. In contrast, samples with high BET areas (**b**, **c**, **d**, **g**) had D–R surface areas that were even larger than the BET areas. This result is illustrated more clearly in Figure 3 which is a plot of D–R surface area versus BET surface area. This plot is essentially linear but with a slope of ~ 3 as compared to 1. A number of reasons may cause discrepancies between surface areas determined from D–R analysis of high temperature CO_2 adsorption and BET analysis of N_2

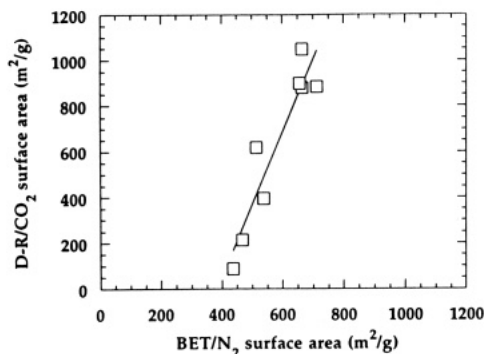


Figure 3. Relationship between BET/N₂ and D-R/CO₂ surface.

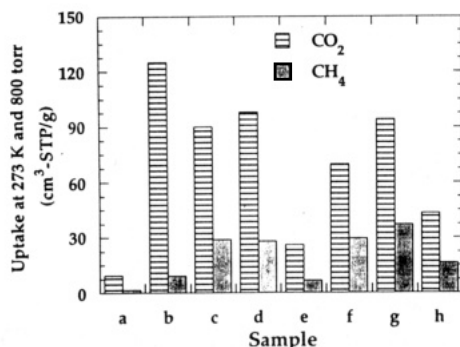


Figure 4. Uptake of CO₂ and CH₄ at 273 K and 800 Torr.

adsorption.¹³ These include (1) activated diffusion such that N₂ does not access all porosity at 77 K, (2) adsorption of CO₂ on only certain adsorption (polar) sites, (3) molecular sieving, (4) molecular size uncertainty, and (5) the basic limitations of the BET and D-R theories as applied to microporous materials. However, it is unclear at this time why a linear relationship between the two different surface areas is observed.

Uptake of carbon dioxide and methane over the pressure range of 0 to 800 Torr has been measured at 273 K for all eight samples. The volumetric uptake of these gases at 800 Torr is presented in Figure 4. A significant variation in uptake of a particular gas is observed for all samples which does not correlate with the BET/nitrogen surface area. The CO₂ uptake correlates with the D-R surface area but this is a direct result of the fact that the D-R area is calculated from the CO₂ isotherms at 273 K. However, the methane uptake varies significantly from sample to sample and does not correlate with either the BET/nitrogen or D-R/carbon dioxide isotherms. This indicates that by changing the BN polymer precursor/processing conditions, significant adsorption selectivity for molecules of similar kinetic diameter may be obtained. We should note that in ultramicroporous materials, observed adsorption selectivity may be a result of kinetic effects rather than molecular sieving and/or adsorption affinity.¹³ By using significantly different adsorption equilibration times, these uptakes might be somewhat higher and result in different relative uptakes for the various gases and BN samples.

In order to determine if the differences in adsorption capacity are related to differences in physical structure, X-ray diffraction (XRD) and small-angle X-ray scattering (SAXS) were measured. The XRD results are reported in Figure 5. All samples show broad peaks indicative of disordered, turbostratic BN. The broad peak around 25° two theta is near the expected peak for hexagonal BN. The shoulder on sample d and the sharp peak on sample e near 30° are in the position expected for B₂O₃. The

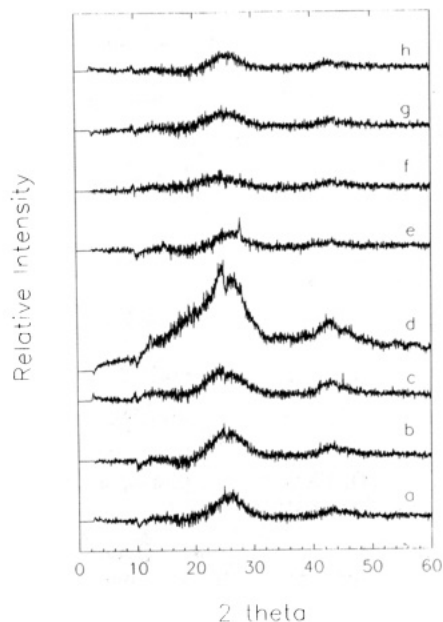


Figure 5. X-ray diffraction results for BN samples.

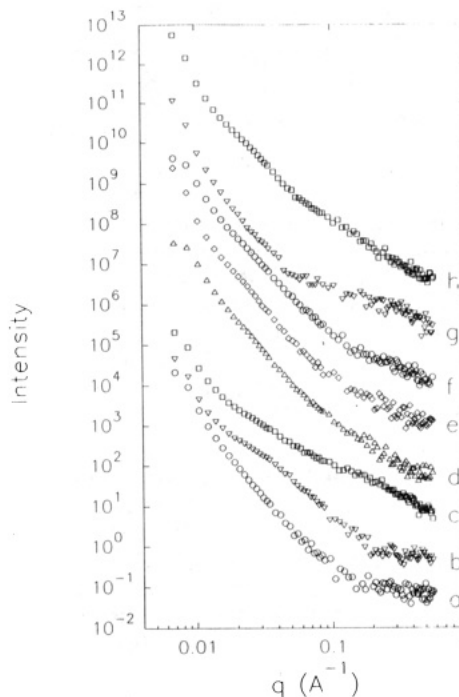


Figure 6. Small angle X-ray scattering (SAXS) intensity versus scattering vector for BN samples.

hump near 44° is also near an expected peak for hexagonal BN. SAXS results are presented in Figure 6 and show significant qualitative differences at both short length scales ($q > 0.1 \text{ \AA}^{-1}$) and intermediate length scales ($0.01 < q < 0.1 \text{ \AA}^{-1}$). The radius of gyration was calculated from scattering at large q , and R_g values between 4 and 9.8 Å were found for the eight samples. We should note that the interpretation of SAXS R_g in microporous materials is problematic since this length scale corresponds to either the size of the solid or pore phases. Also, the absolute magnitude of R_g is less important than relative differences between samples. R_g values are reported in Table 1.

Further information from CO₂ adsorption may be obtained from analysis of the D-R plots. For D-R analysis, the log of the volume adsorbed is plotted versus the square of the log of P_0/P . This plot should be linear if the adsorption potential is described by a Gaussian distri-

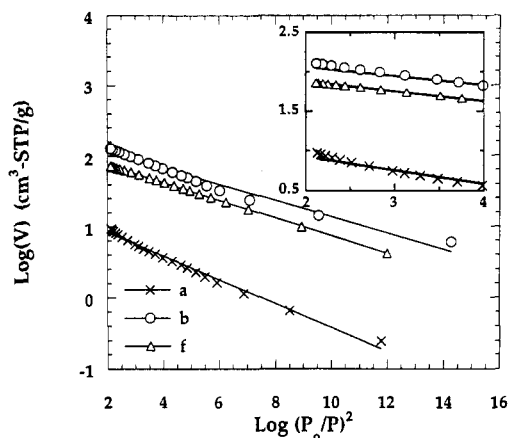


Figure 7. D-R/CO₂ plots for samples a, b, and f showing nonlinearity at higher relative pressure.

Table 1. SAXS Radius of Gyration (R_g) and D-A Exponent Values and Characteristic Energy Obtained from Analysis of CO₂ Adsorption Isotherms at 273 K

sample	R_g (Å)	D-A exponent	D-A energy (kJ/mol)
a	5	1.25	4.5
b	4	1.40	4.2
c	8.4	1.71	2.2
d	9.8	1.97	2.6
e	8.7	2.21	10.1
f	6.6	2.11	10.0
g	5.6	1.81	6.4
h	6.6	1.46	8.3

bution. The surface area is obtained by extrapolating to $\log(P_0/P)^2$ equal to zero. For some materials, this plot is not linear and this is attributed to nonuniform pore size and/or a heterogeneous adsorption surface energy. Typical D-R plots are shown in Figure 7 which shows both a sample which is linear (f) and two samples which have nonlinear D-R plots (a, b). All samples which exhibited nonlinear behavior exhibited type C behavior as classified by Marsh and Rand.¹⁴

The Dubinin-Astakov (D-A) adsorption model allows the coefficient of $\log(P_0/P)$ to vary instead of being fixed at a value of 2. The value of this coefficient was determined for each sample and is reported in Table 1. Values of the D-A coefficient varied significantly from 2 for certain samples and reflect differences in the shape of the adsorption potential-pore volume distribution. It is interesting to note that the range of the D-K coefficients that we observe (1.25–2.21) is very similar to the range of 1.1 to 2 for microporous carbons of various degrees of activation.¹⁵ In general, the value of the D-A exponent varies between 1 and 3 with values approaching 3 for micropores of a small size range and approaching 1 for a broad range of pore sizes/adsorption potential.¹⁶ Also included in Table 1, are the characteristic adsorption energies obtained from the D-A adsorption model. No correlation between this adsorption energy and structural and/or adsorption properties is observed. This is in contrast to previous work with carbons which demonstrated a positive relationship between adsorption energy and SAXS.¹⁶

Figure 8 is a plot of the selectivity of CH₄ as compared to CO₂ versus the D-A exponent obtained from CO₂ adsorption. Here, we define selectivity as the methane uptake at 800 Torr and 273 K divided by the uptake of

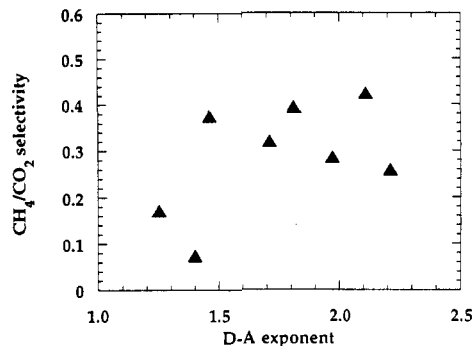


Figure 8. Variation of CH₄/CO₂ selectivity at 273 K and 800 Torr as a function of the D-A/CO₂ adsorption isotherm exponent.

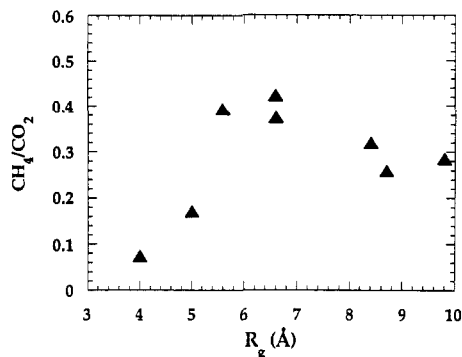


Figure 9. Variation of CH₄/CO₂ selectivity at 273 K and 800 Torr as a function of the SAXS radius of gyration, R_g .

CO₂ at the same conditions. For samples with a D-A exponent near 2, the selectivity is approximately the same between the different samples. However, for samples with a D-A exponent much less than 2, significant changes in selectivity are noted. There appears to be a much better correlation between selectivity and D-A exponent than with either BET/N₂ or D-R/CO₂ surface areas.

Figure 9 is a similar plot to Figure 8 except that the adsorbent selectivity referenced to CO₂ is plotted versus the SAXS-determined radius of gyration, R_g . The selectivity for a particular gas as compared to CO₂ is essentially constant for the samples with R_g greater than ~6 Å; however, the selectivity for methane decreases significantly for the two samples with the smallest R_g value. It is interesting to note that these two samples are a and b which had D-R/CO₂ surface areas which were almost an order of magnitude different.

Conclusions

By variation of the type of polymer precursor and synthesis/pyrolysis conditions in a systematic fashion, the pore structure and adsorption properties of boron nitride can be varied over a fairly wide range. Differences in adsorption behavior can be linked to differences in the microporous nature of these adsorbents as determined from both SAXS and D-A analysis of CO₂ adsorption isotherms at 273 K. However, neither the D-A characteristic adsorption energy or the surface area (either BET/N₂ or D-R/CO₂) was related to the observed adsorption behavior.

Acknowledgment. This work has been supported by the UNM/NSF Center for Micro-Engineered Ceramics which is funded by NSF (CDR-8803512), Sandia and Los Alamos National Laboratories, the New Mexico Research and Development Institute, and the Ceramics industry.

(14) Marsh, H.; Rand, B. *J. Colloid Interface Sci.* 1970, 33, 101.

(15) János, A.; Stoeckli, H. F. *Carbon* 1979, 17, 465.

(16) McEnaney, B. *Carbon* 1987, 25, 69.